ADVANCES IN ATMOSPHERIC SCIENCES, VOL. 36, SEPTEMBER 2019, 1015–1026

• **Review** •

Recent Progress of Aerosol Light-scattering Enhancement Factor Studies in China

Chunsheng ZHAO*[1], Yingli YU[1], Ye KUANG[2], Jiangchuan TAO[2], and Gang ZHAO[1]

[1]*Department of Atmospheric and Oceanic Sciences, School of Physics, Peking University, Beijing* 100871*, China*
[2]*Institute for Environmental and Climate Research, Jinan University, Guangzhou* 510632*, China*

(Received 19 November 2018; revised 27 March 2019; accepted 16 May 2019)

ABSTRACT

Assessment of the radiative forcing of aerosols in models still lacks sufficient input data for aerosol hygroscopicity. The light scattering enhancement factor [$f(\mathrm{RH},\lambda)$] is a crucial parameter for describing aerosol hygroscopic growth properties. In this paper, we provide a survey of $f(\mathrm{RH},\lambda)$ studies in China for the past seven years, including instrument developments of humidified nephelometers, ambient $f(\mathrm{RH},\lambda)$ measurements in China, $f(\mathrm{RH},\lambda)$ parameterization schemes, and $f(\mathrm{RH},\lambda)$ applications in aerosol measurements. Comparisons of different $f(\mathrm{RH},\lambda)$ parameterizations are carried out to check their performance in China using field measurement datasets. We also summary the parameterization schemes for predicting $f(\mathrm{RH},\lambda)$ with aerosol chemical compositions. The recently developed methods to observe other aerosol properties using $f(\mathrm{RH},\lambda)$ measurements, such as calculating the aerosol hygroscopicity parameter, cloud condensation nuclei number concentration, aerosol liquid water content, and aerosol asymmetry factor, are introduced. Suggestions for further research on $f(\mathrm{RH},\lambda)$ in China are given.

Key words: aerosol, hygroscopicity, light-scattering enhancement factor, humidified nephelometer

Citation: Zhao C. S., Y. L. Yu, Y. Kuang, J. C. Tao, and G. Zhao, 2019: Recent progress of aerosol light-scattering enhancement factor studies in China. *Adv. Atmos. Sci.*, **36**(9), 1015–1026, https://doi.org/10.1007/s00376-019-8248-1.

Article Highlights:

- A summary of aerosol light-scattering enhancement factor studies in China is given.
- Newly developed methods for measurement of aerosol microphysical properties are introduced.
- Suggestions for further research in China are given.

1. Introduction

Aerosol optical properties are crucial input parameters for accurate estimation of the direct aerosol radiative forcing in climate models. Assessment of the radiative forcing of aerosols in models still lacks sufficient input data for relative humidity (RH)-dependent aerosol optical properties. Information on aerosol hygroscopicity is always insufficiently implemented in climate models.

Usually, long-term measurements of aerosol optical properties are performed under dry conditions (RH < 30%–40%) in order to keep measurements comparable, as recommended by WMO (World Meteorological Organization)/GAW (Global Atmosphere Watch) (2003). Most aerosol particles may change in size owing to their water uptake ability (hygroscopicity) as RH increases. This RH effect of ambient aerosols is extremely important for aerosol radiative forcing, atmospheric chemistry, and for the correction of remotely sensed aerosol [e.g. lidar, MAX-DOAS (Multi-Axis Differential Optical Absorption Spectroscopy), or satellite retrieval) with in-situ measurements. The software package OPAC (Optical Properties of Aerosols and Clouds) provides aerosol optical properties in the solar and terrestrial spectral range. However, OPAC provides information on the uptake of water by aerosol particles at eight RH points only (10%, 50%, 70%, 80%, 90%, 95%, 98%, 99%), which is insufficient for the changeable atmospheric environment. AERONET provides long-term observations of ambient aerosol scattering or absorption properties, which are the result of total integration from the ground to the top of the atmosphere. However, as the ambient RH in the vertical direction varies greatly, it is hard to determine the variations of aerosol optical properties under specific RH conditions.

The light scattering enhancement factor $f(\mathrm{RH},\lambda)$, defined as the ratio of the light scattering coefficient (σ_{sp}) observed under elevated RH conditions to that under corresponding dry conditions, is a crucial parameter for describing aerosol hy-

* Correspondence author: Chunsheng ZHAO
Email: zcs@pku.edu.cn

groscopic growth properties:

$$f(\mathrm{RH},\lambda) = \frac{\sigma_{\mathrm{sp}}(\mathrm{RH},\lambda)}{\sigma_{\mathrm{sp}}(\mathrm{RH}_{\mathrm{dry}},\lambda)}\,, \tag{1}$$

where the scattering coefficient $\sigma_{\mathrm{sp}}(\mathrm{RH},\lambda)$ depends on the wavelength λ and the RH. It is important to include $f(\mathrm{RH},\lambda)$ when deriving related optical properties, like the single scattering albedo and aerosol asymmetry factor at ambient conditions for aerosol radiative forcing.

Pilat and Charlson (1966) were the first to measure the aerosol light scattering enhancement factor, with a tandem integrating nephelometer. In a subsequent study, Covert et al. (1972) introduced a measuring method to determine the $f(\mathrm{RH},\lambda)$ at a set RH value with a humidified integrating nephelometer. More recently, the principle of humidified nephelometer has been improved by increasing the number of nephelometers (Koloutsou-Vakakis et al., 2001), increasing the number of water baths (Liu and Zhao, 2016), and developing a method of conditioning the aerosol sample to vary the RH (Convert et al., 1972; Day et al., 2000). By adding a fast temperature and RH feedback controller to the humidified nephelometer and maintaining a stable reference RH, a quick, automated response of the scanned RH, and $f(\mathrm{RH},\lambda)$ measurement, can be achieved.

Several comprehensive review papers (e.g., Kreidenweis et al., 2014; Titos et al., 2016) serve as good references for nephelometry techniques used worldwide, as well as $f(\mathrm{RH},\lambda)$ measurements and the various $f(\mathrm{RH},\lambda)$ parameterizations in existence. Here, we provide a survey of $f(\mathrm{RH},\lambda)$ studies in China for the past seven years, including instrument developments of humidified nephelometers, ambient $f(\mathrm{RH},\lambda)$ measurements in China, $f(\mathrm{RH},\lambda)$ parameterization schemes, and $f(\mathrm{RH},\lambda)$ applications in aerosol measurements.

2. Instrumentation development in China

Yan et al. (2009) were the first Chinese group to build a humidified nephelometer. Unfortunately, the temporal resolution of the system was low, with a 3-h sampling time for RH scan measurements. Subsequently, similar humidified nephelometer devices were developed, by Chen et al. (2014), Liu et al. (2014), Zhang et al. (2015), and Wu et al. (2017). Thus far, the variation in RH of the aerosol sample has been achieved by a single water bath, with the RH points of $f(\mathrm{RH},\lambda)$ cycles ranging from about 50% to about 90%. One cycle costs about 90 min, because after each cycle of 45 min has finished, the water bath needs about another 45 min to cool.

In order to study the diurnal variations of aerosol hygroscopic properties in North China, Liu and Zhao (2016) designed a new humidified nephelometer system with the advantage of high temporal resolution and high humidification efficiency (Fig. 1). In this system, two water baths are used for the first time in China to control the humidification process in turn, reducing the circulation cycle from 2–3 h to about 1 h. Besides, the used TSI 3563 nephelometer lamp power was reduced from 75 W to 25 W, and a piece of the heat mirror is set ahead of the lamp for the TSI 3563 nephelometer. Owing to these modifications, the temperature rising inside the chamber decreases from 4.3°C to 2.3°C, and the humidification efficiency rises. The original RH sensor inside the chamber was inaccurate, so two Vaisala sensors were placed at the inlet and outlet of the nephelometer to correct the RH inside the chamber.

Kuang et al. (2017) improved the humidified nephelometer developed by Liu and Zhao (2016) with a control system. The corresponding temporal resolution of $f(\mathrm{RH},\lambda)$ cycles was about 45 min or even less, depending mostly on the scanned RH range. The advantage of this improved device is its high temporal resolution, meaning it can be used in studies of highly polluted regions where diurnal variations of aerosol properties are significant.

3. Ambient measurements of $f(\mathrm{RH},\lambda)$ in China

In-situ characterization of aerosol optical properties provides a uniquely detailed means of evaluating the fundamental physicochemical characteristics of aerosols. It helps to ac-

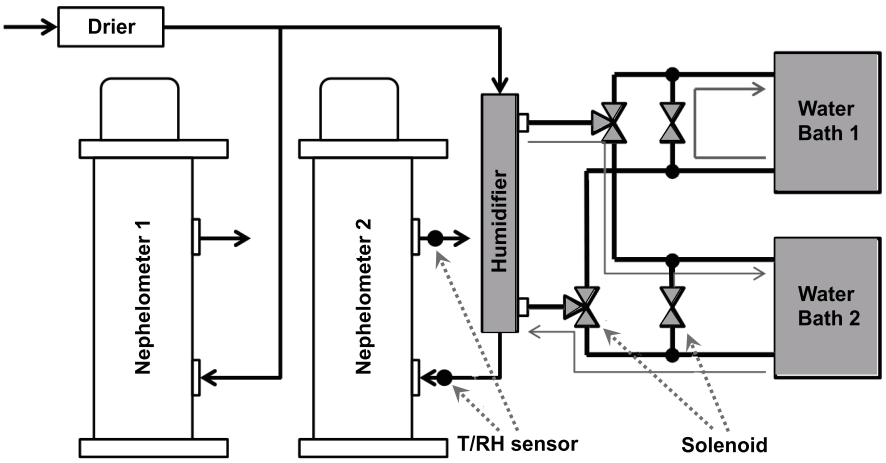

Fig. 1. A new humidified nephelometer system designed by Liu and Zhao (2016).

curately determine the key climate-relevant parameters, such as the single scattering albedo at different wavelengths and RH conditions. In-situ measurements of aerosol scattering coefficients are usually performed at RH below 30%–40% (WMO/GAW, 2003). $f(\mathrm{RH},\lambda)$ measurements bridge the gap of in-situ aerosol optical measurements between dry and ambient conditions. This is important for comparison and validation of remote sensing and visibility studies, with large datasets of in-situ measurements carried out globally. Recently, numerous $f(\mathrm{RH},\lambda)$ measurements have been conducted in China, especially in the North China Plain (NCP), Yangtze Delta, and Pearl River Delta regions.

The NCP is one of the most polluted regions in China. Liu et al. (2013) calculated the average $f(80\%,525)$ was 1.97 during the summer (20–27 September) of 2011 at a site located in the northwest of Beijing at Peking University. Besides, measurements taken during the summer (17 June to 16 August) of 2014 at Raoyang showed that the average $f(80\%,520)$ and $f(85\%,520)$ was 2.28 and 3.39, respectively. These high $f(\mathrm{RH},\lambda)$ values at this site are because of high concentrations of secondary inorganic components (Wu et al., 2017). Yang et al. (2015) showed that the average $f(80\%,550)$ was 1.97 during autumn (5 October to 2 November) of 2014 at a site located in the north of Beijing city at Beijing Normal University. Qi et al. (2018) reported measurements from Gucheng, Hebei Province, during winter (17–22 December) of 2016 and showed that the average values of $f(80\%,450)$, $f(80\%,550)$ and $f(80\%,700)$ were 1.27, 1.29 and 1.32, respectively. The measurements of $f(\mathrm{RH},\lambda)$ introduced in Yu et al. (2018) were adopted here. Results illustrated that the average $f(80\%,525)$ during autumn (18 October to 25 November) of 2016 at Gucheng, Hebei Province, was 1.41. The average $f(80\%,525)$ in a downtown Beijing site during spring (25 March to 9 April) of 2017 was 1.60. The aerosol hygroscopicity at Zhangqiu, Shandong Province, was measured during summer (19 July to 25 August) of 2017, and the results showed that the average $f(80\%,525)$ during the observation period was 1.74. Zhao et al. (2018b) conducted $f(\mathrm{RH},\lambda)$ measurements in three seasons (12 January to 14 February for winter, 6 July to 21 August for summer, and 30 September to 13 November for autumn) at a downtown Beijing site in 2017, and their results showed that the average values of $f(80\%,525)$ during these three seasons were 1.47, 1.54 and 1.53, respectively. Lin'an is a regional background station located in the Yangtze Delta region. At this site, measurements conducted in the spring (1–31 March) of 2013 showed the average values of $f(85\%,450)$, $f(85\%,550)$ and $f(85\%,700)$ to be 1.51, 1.58 and 1.59, respectively (Zhang et al., 2015). Measurements in Guangzhou, located in the Pearl River Delta region, during winter (8–15 December) of 2013 showed that the average of $f(80\%,525)$ was 1.58 (Deng et al., 2016). Liu et al. (2018) reported that the average $f(80\%,525)$ in Guangzhou was 1.77 during the spring (22 February to 18 March) of 2014.

In most of these cases, the $f(\mathrm{RH},\lambda)$ increases continuously and monotonically under conditions of increasing RH. However, Kuang et al. (2016) found jump phenomena in the $f(\mathrm{RH},\lambda)$ can be frequently observed, indicating the deliquescent phenomena of ambient aerosols in the NCP. The observed deliquescent phenomena of ambient aerosols exhibit distinct diurnal patterns and are highly correlated with ammonium sulfate. The frequently observed deliquescent phenomena of ambient aerosols implies that current parameterization schemes that describe the RH dependence of particle light scattering may result in a significant bias when estimating aerosol effects on climate.

A summary of $f(\mathrm{RH},\lambda)$ measurements in China is given in Fig. 2. We can see that $f(\mathrm{RH},\lambda)$ varies substantially among different sites and seasons in China. Such significant variations are due to the varying pollution emission patterns, chemical compositions, and particle number size distributions (PNSDs).

4. $f(\mathrm{RH},\lambda)$ parameterizations

Many equations have been proposed to describe $f(\mathrm{RH},\lambda)$ (Titos et al., 2016). These equations can be divided into three categories according to the number of fitting parameters: single-parameter equations, two-parameter equations, and three-parameter equations. The single-parameter schemes are:

$$f(\mathrm{RH}) = (1-\mathrm{RH})^{-\gamma}\,, \tag{2}$$

$$f(\mathrm{RH}) = \left(\frac{1-\mathrm{RH}}{1-\mathrm{RH}_0}\right)^{-\gamma}\,, \tag{3}$$

$$f(\mathrm{RH}) = \left(1+a\frac{\mathrm{RH}}{1-\mathrm{RH}}\right)^{7/3}\,, \tag{4}$$

$$f(\mathrm{RH}) = 1+\kappa_{\mathrm{sca}}\frac{\mathrm{RH}}{1-\mathrm{RH}}\,. \tag{5}$$

Parameterization Eqs. (2)–(5) were proposed by Kasten (1969), Sheridan et al. (2002), Fierz-Schmidhauser et al. (2010) and Brock et al. (2016), respectively. Parameter γ, a or κ_{sca} describes the variations of aerosol scattering with RH. As the reference RH in the dry condition RH_0 is not zero when measuring $f(\mathrm{RH},\lambda)$, according to Eq. (5), Kuang et al. (2017) suggested that the measured $f(\mathrm{RH},\lambda)$ should be fitted by:

$$f(\mathrm{RH}) = \left(1+\kappa_{\mathrm{sca}}\frac{\mathrm{RH}}{1-\mathrm{RH}}\right)\Big/\left(1+\kappa_{\mathrm{sca}}\frac{\mathrm{RH}_0}{1-\mathrm{RH}_0}\right)\,. \tag{6}$$

In order to describe measured $f(\mathrm{RH},\lambda)$ cycles more precisely, different two-parameter schemes were further introduced by Hänel (1981), Chen et al. (2014), and Kotchenruther and Hobbs (1998):

$$f(\mathrm{RH}) = c(1-\mathrm{RH})^{-\gamma}\,, \tag{7}$$

$$f(\mathrm{RH}) = c(1-\mathrm{RH})^{-\gamma\mathrm{RH}}\,, \tag{8}$$

$$f(\mathrm{RH}) = 1+a\mathrm{RH}^{b}\,. \tag{9}$$

where parameter c indicates the intercept of $f(\mathrm{RH},\lambda)$ cycles when RH = 0%. Parameter b, cooperated with parameter a, determines the variations of scattering with RH.

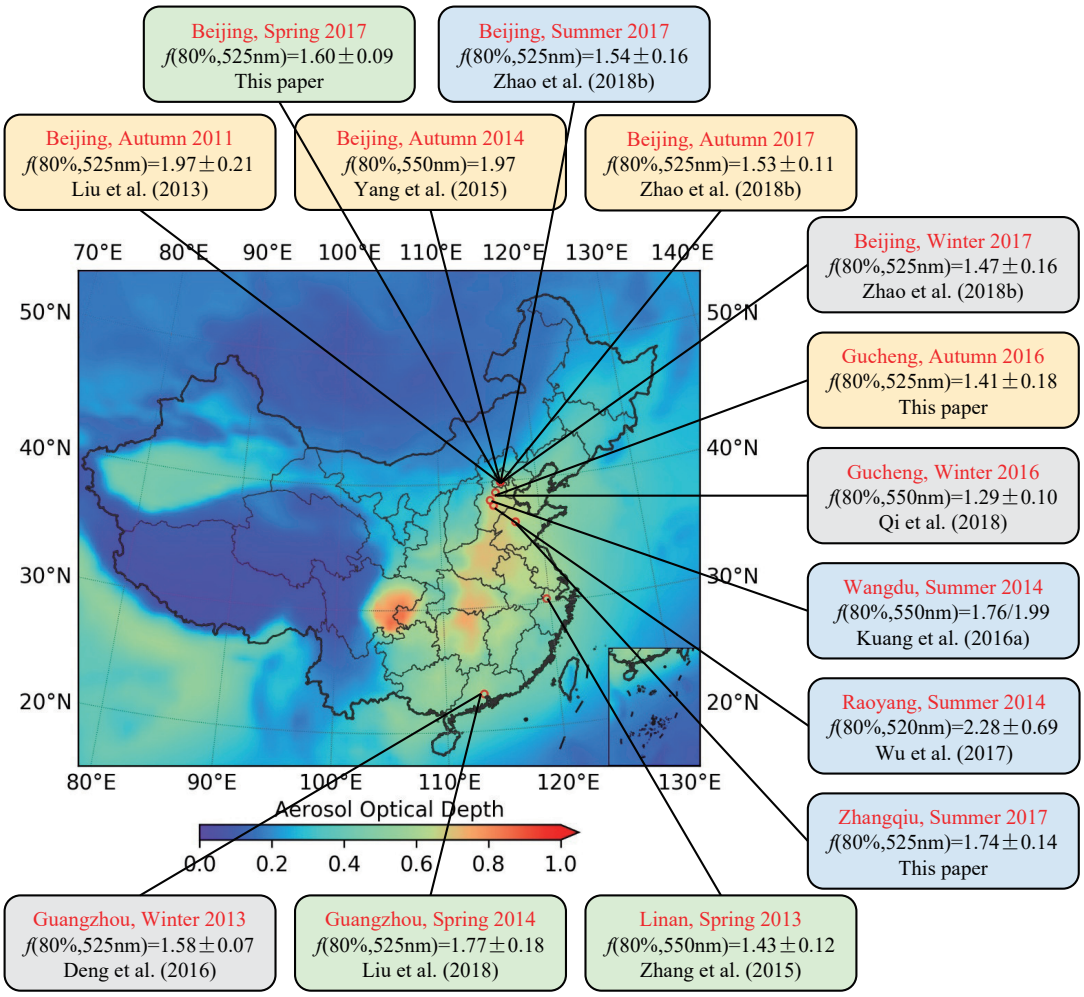

Fig. 2. Summary of $f(\mathrm{RH},\lambda)$ related measurements in China over the past seven years. The different background colors of the boxes indicate the different measurement seasons. Green means spring, blue means summer, yellow means autumn, and grey means winter.

Furthermore, there have been many schemes with more parameters proposed to represent $f(\mathrm{RH},\lambda)$ cycles (Kotchenruther et al., 1999; Day et al., 2000; IMPROVE, 2000; Koloutsou-Vakakis et al., 2001; Sheridan et al., 2001; Nessler et al., 2005; Titos et al., 2016). The three-parameter scheme proposed by IMPROVE (2000) is also applied in China (Yan et al., 2009; Wu et al., 2017):

$$f(\mathrm{RH}) = 1 + A_1\mathrm{RH} + A_2\mathrm{RH}^2 + A_3\mathrm{RH}^3\,, \qquad (10)$$

where parameter A_1, A_2 and A_3 determine the aerosol scattering variations with RH together.

The applications and performances of these equations adopted in China are described in this section.

4.1. *Applications of $f(\mathrm{RH},\lambda)$ parameterizations in China in recent years*

Fitting results in China are described here. One-parameter equations are simple and commonly used. Yu et al. (2018) compared the performances of Eq. (3) and Eq. (6) to fit the measured $f(\mathrm{RH},525)$ curves. The results showed that the deviations of the fitted $f(55\%,525)$, $f(70\%,525)$, $f(85\%,525)$ by Eq. (6) were all within 10%, while the fitted deviations of Eq. (3) can reach 20%, suggesting Eq. (6) should be used to fit $f(\mathrm{RH},\lambda)$ curves.

With additional parameters in the equations, two-parameter equations are introduced to describe $f(\mathrm{RH},\lambda)$ curves more precisely. Yang et al. (2015) used Eq. (9) to fit $f(\mathrm{RH},550)$ curves, and the square of the correlation coefficient (R^2) between the fitted and measured $f(\mathrm{RH},550)$ values was 0.87. Liu et al. (2013) introduced a two-parameter equation, Eq. (9), to fit $f(\mathrm{RH},525)$ curves, and the R^2 between the fitted and measured $f(\mathrm{RH},525)$ values was 0.93. Kuang et al. (2016) proved that $f(\mathrm{RH},550)$ curves without deliquescent phenomena and $f(\mathrm{RH},550)$ curves with RHs higher than deliquescence points, can be fitted well by Eq. (9). Zhang et al. (2015) applied Eq. (7) and Eq. (9) to $f(\mathrm{RH},550)$ curves. The fitted parameters of Eq. (7) and Eq. (9) changed along with local pollution and dust episodes. For Eq. (7), the results

showed that larger $f(\mathrm{RH},\lambda)$ values resulted in bigger values of parameters c and γ. Moreover, the fitted parameters of the measured $f(\mathrm{RH},550)$ were found to be related to the mass fractions of nitrate. Similarly, Qi et al. (2018) also utilized both Eq. (7) and Eq. (9) to fit measured $f(\mathrm{RH},550)$. The results showed that the R^2 of Eq. (7) was 0.42 and the R^2 of Eq. (9) was 0.35. They found that parameter γ in Eq. (7) was more sensitive to the variations of $f(\mathrm{RH},550)$, and the values of parameters a and b in Eq. (9) grew with the increase in aerosol hygroscopicity. Zhao et al. (2018b) assessed the ability of Eqs. (5), (7), (8) and (9) to describe $f(\mathrm{RH},525)$ curves and, ultimately, according to the calculated R^2 between the fitted and measured $f(\mathrm{RH},525)$ values, Eq. (8) was selected to fit $f(\mathrm{RH},525)$ curves. In winter, the R^2 values between the fitted and measured $f(\mathrm{RH},525)$ values were 0.88, 0.88 and 0.89 under very clean, moderately clean and polluted conditions, respectively. Meanwhile, the R^2 values were 0.89, 0.94 and 0.96 for summer, but 0.89, 0.94 and 0.98 for autumn, respectively.

Deng et al. (2016) and Wu et al. (2017) both utilized the three-parameter Eq. (10) to fit measured $f(\mathrm{RH},525)$ and $f(\mathrm{RH},520)$ curves, respectively. All the fitting results are illustrated in detail in Table 1.

4.2. *Comparisons of different* $f(\mathrm{RH},\lambda)$ *parameterizations*

In order to access the ability of these proposed parameterizations to fit $f(\mathrm{RH},\lambda)$ curves, the curves of $f(\mathrm{RH},450)$, $f(\mathrm{RH},525)$ and $f(\mathrm{RH},635)$ measured at Gucheng in 2016 and illustrated in Yu et al. (2018) and Zhangqiu in 2017, expressed in section 3, are also introduced here. The fitting results of the data from Gucheng and Zhangqiu are illustrated in Tables 2 and 3, respectively. The two-parameter equations can better express $f(\mathrm{RH},\lambda)$ curves than the single-parameter equations, while the three-parameter equation does not show any obvious advantage.

As shown in Table 2, for the Gucheng data introduced in Yu et al. (2018), Eq. (8) describes the $f(\mathrm{RH},\lambda)$ curves with the highest R^2 and lowest root-mean-square error (RMSE) for all three wavelengths. The corresponding R^2 values at 450 nm, 525 nm and 635 nm are 0.993, 0.994 and 0.995, respectively. The R^2 values of the three-parameter Eq. (10) at 450 nm, 525 nm and 635 nm are 0.990, 0.991 and 0.992, respectively, which are lower than those of Eq. (7) or (8). The R^2 values of single-parameter schemes are the smallest, but still higher than 0.92. Equation (5) is the best single-parameter equation, with corresponding R^2 values at 450 nm, 525 nm and 635 nm of 0.975, 0.974 and 0.972, respectively.

Table 3 shows that, for the data from Zhangqiu, Eq. (10) is the best, and the R^2 of the two-parameter schemes is larger than that of the single-parameter schemes. For the single-parameter schemes, the R^2 values are all higher than 0.92, and Eq. (3) is the best single-parameter scheme, with R^2 values of 0.970, 0.967 and 0.970 at 450 nm, 525 nm and 635 nm, respectively. For the two-parameter schemes, the R^2 values are all higher than 0.98. Equation (7) is proven to be the best, and the R^2 values at 450 nm, 525 nm and 635 nm are 0.988, 0.989 and 0.989, respectively.

The observation sites at Gucheng and Zhangqiu are both in the NCP, surrounded by farmland and residential areas. The degree of pollution at these two sites is severe. As the dataset from Gucheng was collected during autumn and the dataset from Zhangqiu was collected during summer, these selected two datasets represent the background conditions of the NCP in different seasons. Therefore, conclusions drawn from these two datasets have a certain applicability in the NCP, but not all locations in China. As for other locations in China, further studies are needed to evaluate the performance of different fitting equations.

5. Parameterizing $f(\mathrm{RH},\lambda)$ with aerosol chemical compositions

Since the application of the humidification nephelometer system is still limited to the laboratory and intensive measurements in the atmosphere, there is not a large amount of continuous $f(\mathrm{RH},\lambda)$ observation data on a global scale. Therefore, it is necessary to use some other parameters related to $f(\mathrm{RH},\lambda)$ to estimate the $f(\mathrm{RH},\lambda)$ values. Chemical compositions determine the aerosol hygroscopicity and refractive index, which in turn have an important influence on $f(\mathrm{RH},\lambda)$. Numerous studies have been conducted based on in-situ data and laboratory data to explore the relationship between $f(\mathrm{RH},\lambda)$ and aerosol chemical components (Malm et al., 2005; Baynard et al., 2006; Garland et al., 2007; Wang et al., 2007; Pan et al., 2009; Titos et al., 2014; Zieger et al., 2014).

5.1. *Parameterizing* $f(\mathrm{RH},\lambda)$ *at a certain RH with aerosol chemical compositions*

Zhang et al. (2015) sought the relationships between $f(\mathrm{RH},\lambda)$ and the mass fraction of organic matter (OM) (F_{org}) or inorganic matter (F_{io}). Results showed that the statistical relationship between $f(85\%,550)$ and F_{org} was $f(85\%,550) = (2.05 \pm 0.02) - (1.20 \pm 0.04)F_{\mathrm{org}}$, while the statistical relationship between $f(85\%,550)$ and F_{io} was $f(85\%) = (1.10 \pm 0.01) + (0.96 \pm 0.02)F_{\mathrm{io}}$. The study of Wu et al. (2017) indicated that $f(80\%,520)$ increased with an increase in secondary inorganic aerosols mass fraction (F_{sia}), and the R between them was 0.758. The corrsponding statistical relaitionship was calculated to be $f(80\%,520) = 0.981 + 3.502F_{\mathrm{sia}}$. Meanwhile, $f(80\%,520)$ decreased with an increase in F_{org}, with an R of −0.679, and the relationship was $f(80\%,520) = 2.813 - 1.955F_{\mathrm{org}}$. Qi et al. (2018) quantified the relationship between $f(80\%,550)$ and different aerosol chemical compositions. The results showed that $f(80\%,550)$ was negatively related to OM, and the R^2 between them was 0.55. The calculated relationship was found to be $f(80\%,550) = -(0.99 \pm 0.12)F_{\mathrm{org}} + (1.70 \pm 0.05)$. The $f(80\%,550)$ was also positively correlated with F_{io} or the nitrate mass fraction (F_{ni}), and the R^2 between both was 0.70. The corresponding relationships were $f(80\%,550) = (1.36 \pm 0.12)F_{\mathrm{io}} + (0.82 \pm 0.05)$ and $f(80\%,550) = (2.465 \pm 0.217)F_{\mathrm{ni}} + (1.027 \pm 0.024)$.

Table 1. Detailed measurement information, including $f(80\%)$ values, wavelengths (WL), sites, time periods, reference RH values, fitting equations, and the fitted parameters. The $f(80\%)$ values noted with "(un)" or "(de)" means that they are from the $f(\mathrm{RH},\lambda)$ curve without or with deliquesce phenomenan. VC, MC, P, LP, NP or DI following the equation number means that the $f(\mathrm{RH},\lambda)$ curves were measured from very clean, moderately clean, polluted, locally polluted, northerly polluted or dust-influenced conditions.

$f(80\%)$	WL (nm)	Site	Time	$\mathrm{RH_{dry}}$	Equation	Parameters	Reference
1.97 ± 0.21	525	Beijing	2011 Au	$\leqslant 30\%$	(9)	$a = 4.34 \pm 0.43$ $b = 6.72 \pm 0.40$	Liu et al. (2013)
2.28 ± 0.69	520	Raoyang	2014 Su	$< 40\%$	(10)	A1 = 0.905, A2 = −0.023 A3 = 0.060	Wu et al. (2017)
1.97	550	Beijing	2014 Au	–	(9)	$a = 3.79$ $b = 6.10$	Yang et al. (2015)
1.76 (un)	550	Wangdu	2014 Su	$< 30\%$	(9)	–	Kuang et al. (2016)
1.99 (de)	550	Wangdu	2014 Su	$< 30\%$	(9)	–	
1.27 ± 0.09	450	Gucheng	2016 Wi	$< 30\%$	–	–	Qi et al. (2018)
1.29 ± 0.10	550	Gucheng	2016 Wi	$< 30\%$	(7)	$c = 0.91 \pm 0.01$ $\gamma = 0.21 \pm 0.01$	
					(9)	$a = 0.56 \pm 0.02$ $b = 3.44 \pm 0.99$	
1.32 ± 0.12	700	Gucheng	2016 Wi	$< 30\%$	–	–	
1.47 ± 0.16	525	Beijing	2017 Wi	$< 30\%$	(8) VC	$c = 0.930$, $\gamma = 0.329$	Zhao et al. (2018b)
					(8) MC	$c = 0.971$, $\gamma = 0.372$	
					(8) P	$c = 0.988$, $\gamma = 0.356$	
1.54 ± 0.16	525	Beijing	2017 Su	$< 30\%$	(8) VC	$c = 0.972$, $\gamma = 0.355$	
					(8) MC	$c = 0.980$, $\gamma = 0.362$	
					(8) P	$c = 0.984$, $\gamma = 0.371$	
1.53 ± 0.11	525	Beijing	2017 Au	$< 30\%$	(8) VC	$c = 0.979$, $\gamma = 0.334$	
					(8) MC	$c = 1.002$, $\gamma = 0.344$	
					(8) P	$c = 1.014$, $\gamma = 0.332$	
1.58 ± 0.07	525	Guangzhou	2013Wi	$< 40\%$	(10)	A1 = 0.731, A2 = 0.138 A3 = 0.007	Deng et al. (2016)
1.77 ± 0.18	525	Guangzhou	2014 Sp	$< 40\%$	(7)	$c = 0.66$, $\gamma = 0.63$	Liu et al. (2018)
1.43 ± 0.12	550	Linan	2013 Sp	$< 40\%$	(7) LP	$c = 0.85 \pm 0.08$ $\gamma = 0.29 \pm 0.04$	Zhang et al. (2015)
					(7) NP	$c = 0.93 \pm 0.07$ $\gamma = 0.28 \pm 0.03$	
					(7) DI	$c = 0.87 \pm 0.05$ $\gamma = 0.27 \pm 0.02$	
					(9) LP	$a = 1.24 \pm 0.29$ $b = 5.46 \pm 1.90$	
					(9) NP	$a = 1.20 \pm 0.21$ $b = 3.90 \pm 1.27$	
					(9) DI	$a = 1.02 \pm 0.19$ $b = 4.51 \pm 0.80$	

Table 2. Fitting results from Gucheng with different fitting equations. The equation number is followed by the fitting parameters in their corresponding equation. Text in red, green and blue represents results at 635 nm, 525 nm and 450 nm, respectively.

Eq (Parameter)	Parameter1	Parameter2	Parameter3	R^2	RMSE	$f(80\%)$
(2) (γ)	0.199 ± 0.072	–	–	0.935	0.094	1.393 ± 0.166
	0.203 ± 0.084			0.938	0.095	1.411 ± 0.183
	0.203 ± 0.084			0.923	0.108	1.402 ± 0.196
(3) (γ)	0.216 ± 0.083	–	–	0.950	0.083	
	0.225 ± 0.090			0.953	0.083	
	0.221 ± 0.096			0.942	0.095	
(4) (a)	0.033 ± 0.012	–	–	0.955	0.054	
	0.034 ± 0.013			0.957	0.056	
	0.034 ± 0.014			0.960	0.057	
(5) (κ_{sca})	0.089 ± 0.039	–	–	0.972	0.045	
	0.093 ± 0.042			0.974	0.045	
	0.092 ± 0.045			0.975	0.051	
(6) (κ_{sca})	0.093 ± 0.046	–	–	0.971	0.044	
	0.098 ± 0.051			0.973	0.044	
	0.097 ± 0.054			0.975	0.048	
(7) (c, γ)	0.829 ± 0.042	0.320 ± 0.085	–	0.993	0.021	
	0.830 ± 0.043	0.327 ± 0.094		0.993	0.022	
	0.863 ± 0.066	0.339 ± 0.104		0.992	0.026	
(8) (c, γ)	0.940 ± 0.039	0.370 ± 0.053	–	0.995	0.019	
	0.945 ± 0.037	0.304 ± 0.087		0.994	0.020	
	1.035 ± 0.067	0.316 ± 0.096		0.993	0.023	
(9) (a, b)	1.293 ± 0.449	5.512 ± 1.532	–	0.991	0.024	
	1.334 ± 0.498	5.451 ± 1.605		0.990	0.027	
	1.433 ± 0.540	6.050 ± 2.051		0.989	0.030	
(10) (A1, A2, A3)	1.106 ± 0.712	-4.112 ± 2.245	4.210 ± 1.918	0.992	0.023	
	1.184 ± 0.785	-4.342 ± 2.471	4.414 ± 2.127	0.991	0.025	
	1.198 ± 0.828	-4.549 ± 2.615	4.639 ± 2.275	0.990	0.029	

5.2. *Parameterizing the fitted parameters of $f(\mathrm{RH}, \lambda)$ with aerosol chemical compositions*

Section 5.1 represents the calculated relationships between $f(\mathrm{RH}, \lambda)$ at a fixed RH condition with aerosol chemical compositions. However, it is critical to obtain the aerosol scattering properties at any RH condition to calculate the ambient aerosol optical properties. As the $f(\mathrm{RH}, \lambda)$ curves are usually described by some appropriate equations, several studies have been carried out to explore the relationships between aerosol chemical compositions and the fitted parameters of $f(\mathrm{RH}, \lambda)$. Zhang et al. (2015) employed the method of Quinn et al. (2005) to study the relationship between F_{org} and the parameter γ in Eq. (3), where the F_{org} was calculated by $F_{org} = \mathrm{OM}/(\mathrm{OM} + \mathrm{SO}_4^{2-})$. The resulting statistical relationship was $\gamma = -0.25F_{org} + 0.48$. However, this scheme is only applicable to the aerosol types dominated by sulfates and organics, and the R^2 between γ and F_{org} was only 0.14. A further study by Zhang et al. (2015) found that nitrate also made an important contribution to the hygroscopic growth of aerosol. The statistical relationship was $\gamma = -0.26F_{org} + 0.50$, and the R^2 between F_{org} and γ was 0.56 when the F_{org} was described as $F_{org} = \mathrm{OM}/(\mathrm{OM} + \mathrm{SO}_4^{2-})$. Furthermore, if the F_{org} was set as $F_{org} = \mathrm{OM}/(\mathrm{OM} + \mathrm{SO}_3^{-} + \mathrm{SO}_4^{2-})$, the relationship was $\gamma = -0.42F_{org} + 0.54$ and the R^2 between F_{org} and γ was 0.68.

Yu et al. (2018) newly proposed a scheme to bridge the gap between aerosol chemical compositions and $f(\mathrm{RH}, \lambda)$ through Eq. (5). They first linked the aerosol hygroscopicity parameter κ and chemical compositions with three dominant inorganic ions ($\mathrm{NH}_4^+, \mathrm{NO}_3^-, \mathrm{SO}_4^{2-}$) and OM. Then, the relationship among κ, the fitted parameter κ_{sca} of $f(\mathrm{RH}, \lambda)$, and the scattering Ångström exponent (SAE), which represents the size of aerosol, was established. Thus, the hygroscopic parameter κ can be determined through aerosol chemical compositions and then the fitted parameter κ_{sca} can be obtained by κ and SAE. The resulting empirical equation to parameterize $f(\mathrm{RH}, \lambda)$ with aerosol chemical compositions is shown as

$$f(\mathrm{RH}, 525) = 1 + (0.01 + 0.70f_{\mathrm{NH_4}} + 0.44f_{\mathrm{NO_3^-}} + 0.62f_{\mathrm{SO_4^{2-}}} + 0.06f_{\mathrm{OM}})(0.45 + 0.15\mathrm{SAE})\frac{\mathrm{RH}}{1 - \mathrm{RH}}. \quad (11)$$

The verification results showed that the correlation coefficient of $f(80\%, 525)$ obtained by observation and parameterization was 0.81. In addition, the method can further consider the influence of the aerosol size on $f(\mathrm{RH}, \lambda)$. This proposed scheme links chemical compositions to $f(\mathrm{RH}, \lambda)$ and can be applied to chemical transport models to reduce assessment errors of aerosol direct radiative forcing and atmospheric visibility.

Table 3. Fitting results from Zhangqiu with different fitting equations. The equation number is followed by the fitting parameters in their corresponding equation. Text in red, green and blue represents results at 635 nm, 525 nm and 450 nm, respectively.

Eq (Parameter)	Parameter1	Parameter2	Parameter3	R^2	RMSE	$f(80\%)$
(2) (γ)	0.327 ± 0.041	–	–	0.970	0.070	1.723 ± 0.112
	0.358 ± 0.058			0.967	0.082	1.741 ± 0.144
	0.358 ± 0.058			0.970	0.094	1.816 ± 0.164
(3) (γ)	0.327 ± 0.043	–	–	0.972	0.055	
	0.359 ± 0.057			0.971	0.064	
	0.397 ± 0.061			0.974	0.072	
(4) (a)	0.058 ± 0.008	–	–	0.922	0.112	
	0.059 ± 0.011			0.921	0.112	
	0.065 ± 0.012			0.932	0.115	
(5) (κ_{sca})	0.168 ± 0.026	–	–	0.949	0.078	
	0.172 ± 0.035			0.949	0.078	
	0.190 ± 0.039			0.959	0.076	
(6) (κ_{sca})	0.179 ± 0.028	–	–	0.947	0.088	
	0.184 ± 0.037			0.947	0.086	
	0.204 ± 0.042			0.958	0.084	
(7) (c, γ)	0.904 ± 0.067	0.397 ± 0.057	–	0.989	0.031	
	0.884 ± 0.072	0.417 ± 0.063		0.989	0.034	
	0.863 ± 0.066	0.458 ± 0.068		0.988	0.039	
(8) (c, γ)	1.057 ± 0.064	0.370 ± 0.053	–	0.987	0.034	
	1.042 ± 0.073	0.389 ± 0.059		0.986	0.037	
	1.035 ± 0.067	0.427 ± 0.063		0.986	0.043	
(9) (a, b)	1.599 ± 0.291	3.408 ± 0.724	–	0.984	0.037	
	1.712 ± 0.335	3.646 ± 0.886		0.985	0.039	
	1.969 ± 0.398	3.805 ± 0.824		0.983	0.047	
(10) (A1, A2, A3)	1.318 ± 0.684	-4.146 ± 2.024	4.559 ± 1.511	0.992	0.026	
	1.307 ± 0.744	-4.282 ± 2.159	4.787 ± 1.625	0.991	0.030	
	1.637 ± 0.795	-5.464 ± 2.412	5.907 ± 1.871	0.989	0.037	

6. Applications of $f(\mathrm{RH}, \lambda)$

$f(\mathrm{RH}, \lambda)$ is an important quantity in its own right, being directly applicable to calculations of visibility and radiative forcing. The $f(\mathrm{RH}, \lambda)$ technique links optical properties of the entire aerosol population and aerosol hygroscopic properties. Recently, most commercial nephelometers tend to be operated with multiple wavelengths—commonly, three. Thus, the humidified nephelometer system can provide rich information on aerosol optics, such as scattering coefficients and backscattering coefficients, at these wavelengths under dry and prescribed RH conditions. This information reflects the change in aerosol volume concentrations, aerosol water uptake ability, and aerosol size distributions due to changes of RH, providing possibilities to calculate some other aerosol microphysical properties based on $f(\mathrm{RH}, \lambda)$ datasets. Here, we introduce recently developed methods to calculate the aerosol hygroscopicity parameter, CCN number concentrations, aerosol liquid water content (ALWC), and aerosol asymmetry factor.

6.1. *Calculating the aerosol hygroscopicity parameter* κ

The RH dependence of the growth of an aerosol particle owing to water uptake can be parameterized in a good approximation by a one-parameter equation—proposed, for example, by Petters and Kreidenweis (2007). The parameter κ is a simple measure of the particle's hygroscopicity and captures all solute properties. Traditionally, an overall hygroscopicity parameter κ can be retrieved from measured $f(\mathrm{RH}, \lambda)$, hereinafter referred to as $\kappa_{f(\mathrm{RH})}$, by combining concurrently measured PNSDs and mass concentrations of black carbon. Kuang et al. (2017) proposed a new method to directly derive $\kappa_{f(\mathrm{RH})}$ based only on measurements from a three-wavelength humidified nephelometer system. The advantage of this newly proposed approach is that $\kappa_{f(\mathrm{RH})}$ can be estimated without any additional information on PNSDs and black carbon. Kuang et al. (2017) verified this method with measurements from different field campaigns conducted in the NCP, and their results demonstrated that this method of deriving $\kappa_{f(\mathrm{RH})}$ is applicable at different sites and in different seasons of the NCP and might also be applicable in other regions around the world. This work directly links $f(\mathrm{RH}, \lambda)$ to κ for the first time, which is a breakthrough for studying the impacts of aerosol hygroscopic growth on aerosol optical properties and connecting aerosol optical properties to aerosol water content. Thus, their results should make the humidified nephelometer system more convenient when it comes to aerosol hygroscopicity research, as well as facilitate other research on the roles of aerosol water in aerosol radiative effects.

6.2. *Calculating ambient ALWC*

Aerosol liquid water plays significant roles in the atmospheric environment, atmospheric chemistry, and climate. Unfortunately, until now, no instruments have been available for real-time monitoring of ambient ALWC. The challenging issue hindering the development of ambient ALWC measurement techniques is that the amount of ambient ALWC is quite small and very sensitive to RH changes, which makes it unable to be measured directly. Kuang et al. (2018) proposed a novel method to calculate ambient ALWC based on measurements of a three-wavelength humidified nephelometer system. The proposed ALWC calculation method includes two steps. The first step is calculating the dry state total volume concentration of ambient aerosol particles, $V_a(\mathrm{RH_{dry}})$, with a machine learning model based on measurements of the "dry" nephelometer. The second step is calculating the volume growth factor $Vg(\mathrm{RH})$ of ambient aerosol particles due to water uptake, using measured $f(\mathrm{RH},\lambda)$ and SAE. Then, ambient ALWC can be derived based on the calculated $V_a(\mathrm{dry})$ and $Vg(\mathrm{RH})$. Kuang et al. (2018) validated the proposed ALWC calculation method using ambient ALWC calculated from the aerosol thermodynamic model of ISORROPIA with measured aerosol chemistry data. Their results demonstrated that a good agreement was achieved between the ALWC calculated from measurements of the humidified nephelometer system and from those estimated using the ISORROPIA model, with a slope and intercept of 1.14 and -8.6 μm^3 cm^{-1} ($R^2 = 0.92$), respectively. The thermodynamic model needs chemistry data as inputs, which requires expensive chemical instruments, and has a relatively low temporal resolution (1 h). The thermodynamic model only accounts for the ALWC contribution from inorganic aerosol components and is unable to take into account that from organic matter. Even when measurements of aerosol organic matter are available, accurate estimation of their hygroscopicity still remains unresolved. The advantage of this newly proposed method is that the required measurement data can be obtained solely from the humidified nephelometer system, which is quite stable and has a high temporal resolution. Also, this method considers the contributions of both inorganic and organic aerosol components to ambient ALWC, facilitating the real-time monitoring of ambient ALWC and promoting the study of aerosol liquid water and its role in atmospheric chemistry, secondary aerosol formation, and climate change.

6.3. *Calculating number concentrations of CCN*

Based on measurements of a humidified nephelometer system, Tao et al. (2018) proposed a new method to calculate the number concentration of CCN (N_{CCN}), which is a key parameter of cloud microphysics and the indirect radiative effect of aerosol. In general, N_{CCN} is directly measured under supersaturated conditions in CCN chambers, which are complex and costly. As accumulation-mode aerosols contribute most to both aerosol optical properties and the aerosol CCN activity, N_{CCN} can be predicted by its relationship with the aerosol scattering coefficient. In this new method, a look-up table that involves the scattering coefficient σ_{sp}, SAE, and hygroscopicity parameter κ, is established to derive N_{CCN} based on measurements of a three-wavelength humidified nephelometer system that can measure the required three parameters (i.e., σ_{sp}, SAE and κ). This method has been validated by comparing the measurements of a humidified nephelometer system and a CCN counter in Gucheng in 2016 (Tao et al., 2018). For the calculated and measured N_{CCN}, good agreements can be achieved. Relative deviations are within 30%, and the slope and R of the regression are 1.03 and 0.966, respectively. Because the humidified nephelometer system is simply operated and stable, the real-time monitoring of N_{CCN}, especially on aircraft, can be facilitated by this new method. Furthermore, this method is more applicable for studies of aerosol–cloud interaction, due to its applicability at lower supersaturations than 0.1%.

6.4. *Calculating the asymmetry factor of aerosol*

In addition to aerosol optical depth and aerosol single-scattering albedo, the aerosol phase function is the most important factor for assessing direct aerosol radiative forcing. However, little attention has been paid to the measurements and parameterization of the asymmetry factor g. Zhao et al. (2018a) proposed a novel method to calculate g based on measurements from the humidified nephelometer system. This method constrains the uncertainty of g within 2.56% for dry aerosol populations and 4.02% for ambient aerosols, where the aerosol hygroscopic growth has been taken into account. The total uncertainty of the calculation of g using the Random Forest machine learning model is 4.47%. Sensitivity studies show that aerosol hygroscopicity plays a vital role in the accuracy of predicting g. This new method for calculating g has been validated by comparing the values of g from the Random Forest machine learning model and those from field-measured phase function Zhao et al. (2018a). The g values with these two methods show good consistency, with 95% of the data within the relative difference of 6.5%.

7. Summary and prospects

This paper reviews the progress in the study of aerosol light-scattering enhancement factor $f(\mathrm{RH},\lambda)$ over the last seven years, including instrumentation development, ambient $f(\mathrm{RH},\lambda)$ measurements over China, $f(\mathrm{RH},\lambda)$ parameterizations, and $f(\mathrm{RH},\lambda)$ applications.

A detailed understanding of the effects of RH on aerosol scattering is important for the development of realistic model parameterizations, but it is gained at the expense of measurement spatial coverage. Table 1 presents a survey of the $f(\mathrm{RH},\lambda)$ measurements performed over the past seven years in China. Field campaigns during the past decade over the polluted region of eastern China have provided valuable observational constraints for the RH effects on aerosol optical properties. Unfortunately, most of these studies focused on polluted environments dominated by urban particles. So

far, we lack $f(\mathrm{RH},\lambda)$ measurements in different environments predominated by other aerosol types, such as dust particles in western China, rural aerosols emitted by agricultural biomass burning activities, and marine aerosols in the coastal or near-coastal marine atmosphere of China. Long-term continuous in-situ measurements of $f(\mathrm{RH},\lambda)$ are as important as measurements of optical and microphysical aerosol particle properties performed under dry conditions through monitoring networks for climate forcing and remote sensing studies. Till now, these studies have been limited by vertical measurements of $f(\mathrm{RH},\lambda)$, but this limitation can be remedied to some extent by utilizing mobile platforms, such as aircraft or tethered balloons. The need for vertical observations of aerosol hygroscopicity is considerable.

The observations discussed in this paper demonstrate the complexity of atmospheric aerosols with regard to hygroscopicity. There are significant diurnal variations of aerosol properties in eastern China, where air pollution events occur frequently. In order to capture the diurnal variation pattern of $f(\mathrm{RH},\lambda)$ in such a rapidly changing environment, a high temporal resolution humidified nephelometer is needed.

Results from several studies indicate that the aerosol hygroscopicity parameter, ALWC, CCN, and aerosol asymmetry factor can be derived based on measurements from the three-wavelength humidified nephelometer system, demonstrating that the humidified nephelometer system and $f(\mathrm{RH},\lambda)$ measurements have broad usage prospects and can be widely used in different atmospheric research areas. The humidified nephelometer system is an optical instrument that has the advantage of stability and easy operation; its use in calculating different properties related to aerosol particles should be further explored to make aerosol measurements more convenient. Given this, it should be discussed that, if functions of currently used nephelometers are enough for aerosol instrumentation, for example, is it necessary to add more detecting wavelengths to the nephelometer?

Accurate parameterization of $f(\mathrm{RH},\lambda)$ in air quality prediction models is critical for the accurate prediction of atmospheric visibility, which in turn is important for public concern, airports, shipping, and so on. $f(\mathrm{RH},\lambda)$ is also an important parameter for accurate estimation of direct aerosol radiative effects. However, the link between aerosol optical properties as expressed in $f(\mathrm{RH},\lambda)$ and the dependence of water content on RH is not straightforward, especially over a large RH range. More studies are needed to better describe $f(\mathrm{RH},\lambda)$ as a function of aerosol properties and RH.

Based on $f(\mathrm{RH},\lambda)$ measurements, Kuang et al. (2016) presented an interesting study of deliquescent phenomena of ambient aerosols in the NCP. Ambient RH may decrease to below 30% in the afternoon, which is lower than the efflorescence RH of ammonium sulfate at 298 K (35% RH) (Martin, 2000). This study implies that, during periods when deliquescent phenomena occur, aged ambient aerosols may recrystallize when the ambient RH drops below the efflorescence RH in the afternoon. The ambient aerosol particles will then remain crystallized and experience a sudden change in size related to water uptake that occurs when the ambient RH reaches the deliquescence RH in the evening. This jump in growth of ALWC exerts significant impacts on aerosol aqueous reactions, radiation, and climate. This phenomenon needs further research in the future.

Acknowledgements. This work was supported by the National Natural Science Foundation of China (Grant No. 41590872).

REFERENCES

Baynard, T., R. M. Garland, A. R. Ravishankara, M. A. Tolbert, and E. R. Lovejoy, 2006: Key factors influencing the relative humidity dependence of aerosol light scattering. *Geophys. Res. Lett.*, **33**, L06813, https://doi.org/10.1029/2005gl024898.

Brock, C. A., and Coauthors, 2016: Aerosol optical properties in the southeastern United States in summer- Part 1: Hygroscopic growth. *Atmospheric Chemistry* and *Physics*, **16**, 4987–5007, https://doi.org/10.5194/acp-16-4987-2016.

Chen, J., C. S. Zhao, N. Ma, and P. Yan, 2014: Aerosol hygroscopicity parameter derived from the light scattering enhancement factor measurements in the North China Plain. *Atmospheric Chemistry and Physics*, **14**, 8105–8118, https://doi.org/10.5194/acp-14-8105-2014.

Covert, D. S., R. J. Charlson, and N. C. Ahlquist, 1972: A study of the relationship of chemical composition and humidity to light scattering by aerosols. *J. Appl. Meteor.*, **11**, 968–976, https://doi.org/10.1175/1520-0450(1972)011<0968:ASOTRO>2.0.CO;2.

Day, D. E., W. C. Malm, and S. M. Kreidenweis, 2000: Aerosol light scattering measurements as a function of relative humidity. *Journal of the Air & Waste Management Association*, **50**, 710–716, https://doi.org/10.1080/10473289.2000.10464103.

Deng, H., H. B. Tan, F. Li, M. F. Cai, P. W. Chan, H. B. Xu, X. Y. Huang, and D. Wu, 2016: Impact of relative humidity on visibility degradation during a haze event: A case study. *Science of the Total Environment*, **569–570**, 1149–1158, https://doi.org/10.1016/j.scitotenv.2016.06.190.

Fierz-Schmidhauser, R., P. Zieger, M. Gysel, L. Kammermann, P. F. DeCarlo, U. Baltensperger, and E. Weingartner, 2010: Measured and predicted aerosol light scattering enhancement factors at the high alpine site Jungfraujoch. *Atmospheric Chemistry and Physics*, **10**, 2319–2333, https://doi.org/10.5194/acp-10-2319-2010.

Garland, R. M., A. R. Ravishankara, E. R. Lovejoy, M. A. Tolbert, and T. Baynard, 2007: Parameterization for the relative humidity dependence of light extinction: Organic-ammonium sulfate aerosol. *J. Geophys. Res.*, **112**, D19303, https://doi.org/10.1029/2006jd008179.

Hänel, G., 1981: An attempt to interpret the humidity dependencies of the aerosol extinction and scattering coefficients. *Atmos. Environ.*, **15**, 403–406, https://doi.org/10.1016/0004-6981(81)90045-7.

IMPROVE, 2000: Spatial and seasonal patterns and temporal variability of haze and its constituents in the United States. Report III. Available online from http://views.cira.colostate.edu/improve/Publications/Reports/2000/2000.htm.

Kasten, F., 1969: Visibility forecast in the phase of precondensation. *Tellus*, **21**, 631–635, https://doi.org/10.3402/tellusa.v21i5.10112.

Koloutsou-Vakakis, S., and Coauthors, 2001: Aerosol proper-

ties at a midlatitude northern hemisphere continental site. *J. Geophys. Res*., **106**, 3019–3032, https://doi.org/10.1029/2000jd900126.

Kotchenruther, R. A., and P. V. Hobbs, 1998: Humidification factors of aerosols from biomass burning in Brazil. *J. Geophys. Res*., **103**, 32 081–32 089, https://doi.org/10.1029/98JD00340.

Kotchenruther, R. A., P. V. Hobbs, and D. A. Hegg, 1999: Humidification factors for atmospheric aerosols off the mid-Atlantic coast of the United States. *J. Geophys. Res*., **104**, 2239–2251, https://doi.org/10.1029/98jd01751.

Kreidenweis, S. M., and A. Asa-Awuku, 2014: 5.13 - Aerosol hygroscopicity: Particle water content and its role in atmospheric processes. *Treatise on Geochemistry*. 2nd ed. H. D. Holland and K. K. Turekian, Eds., Elsevier, 331–361.

Kuang, Y., C. S. Zhao, N. Ma, H. J. Liu, Y. X. Bian, J. C. Tao, and M. Hu, 2016: Deliquescent phenomena of ambient aerosols on the North China Plain. *Geophys. Res. Lett*., **43**, 8744–8750, https://doi.org/10.1002/2016gl070273.

Kuang, Y., C. S. Zhao, J. C. Tao, Y. X. Bian, N. Ma, and G. Zhao, 2017: A novel method for deriving the aerosol hygroscopicity parameter based only on measurements from a humidified nephelometer system. *Atmospheric Chemistry and Physics*, **17**, 6651–6662, https://doi.org/10.5194/acp-17-6651-2017.

Kuang, Y., C. S. Zhao, G. Zhao, J. C. Tao, W. Y. Xu, N. Ma, and Y. X. Bian, 2018: A novel method for calculating ambient aerosol liquid water content based on measurements of a humidified nephelometer system. *Atmospheric Measurement Techniques*, **11**, 2967–2982, https://doi.org/10.5194/amt-11-2967-2018.

Liu, H. J., and C. S. Zhao, 2016: Design of a humidified nephelometer system with high time resolution. *Acta Scientiarum Naturalium Universitatis Pekinensis*, **52**, 999–1004, https://doi.org/10.13209/j.0479-8023.2016.053. (in Chinese with English abstract)

Liu, H. J., and Coauthors, 2014: Aerosol hygroscopicity derived from size-segregated chemical composition and its parameterization in the North China Plain. *Atmospheric Chemistry and Physics*, **14**, 2525–2539, https://doi.org/10.5194/acp-14-2525-2014.

Liu, L., H. B. Tan, S. J. Fan, M. F. Cai, H. B. Xu, F. Li, and P. Chan, 2018: Influence of aerosol hygroscopicity and mixing state on aerosol optical properties in the Pearl River Delta region, China. *Science of the Total Environment*, **627**, 1560–1571, https://doi.org/10.1016/j.scitotenv.2018.01.199.

Liu, X. G., and Coauthors, 2013: Formation and evolution mechanism of regional haze: A case study in the megacity Beijing, China. *Atmospheric Chemistry and Physics*, **13**, 4501–4514, https://doi.org/10.5194/acp-13-4501-2013.

Malm, W. C., D. E. Day, S. M. Kreidenweis, J. L. Collettjr, C. Carrico, G. McMeeking, and T. Lee, 2005: Hygroscopic properties of an organic-laden aerosol. *Atmos. Environ*., **39**, 4969–4982, https://doi.org/10.1016/j.atmosenv.2005.05.014.

Martin, S. T., 2000: Phase transitions of aqueous atmospheric particles. *Chemical Reviews*, **100**, 3403–3454, https://doi.org/10.1021/cr990034t.

Nessler, R., E. Weingartner, and U. Baltensperger, 2005: Adaptation of dry nephelometer measurements to ambient conditions at the jungfraujoch. *Environ. Sci. Technol*., **39**, 2219–2228, https://doi.org/10.1021/es035450g.

Pan, X. L., P. Yan, J. Tang, J. Z. Ma, Z. F. Wang, A. Gbaguidi, and Y. L. Sun, 2009: Observational study of influence of aerosol hygroscopic growth on scattering coefficient over rural area near Beijing mega-city. *Atmospheric Chemistry and Physics*, **9**, 7519–7530, https://doi.org/10.5194/acp-9-7519-2009.

Petters, M. D., and S. M. Kreidenweis, 2007: A single parameter representation of hygroscopic growth and cloud condensation nucleus activity. *Atmospheric Chemistry and Physics*, **7**, 1961–1971, https://doi.org/10.5194/acp-7-1961-2007.

Pilat, M. J., and R. J. Charlson, 1966: Theoretical and optical studies of humidity effects on the size distribution of a hygroscopic aerosol. *J. Rech. Atmos*., **2**, 165–170.

Qi, X. F., and Coauthors, 2018: Aerosol hygroscopicity during the haze red-alert period in December 2016 at a rural site of the North China Plain. *J. Meteor. Res*., **32**, 38–48, https://doi.org/10.1007/s13351-018-7097-7.

Quinn, P. K., and Coauthors, 2005: Impact of particulate organic matter on the relative humidity dependence of light scattering: A simplified parameterization. *Geophys. Res. Lett*., **32**, L22809, https://doi.org/10.1029/2005gl024322.

Sheridan, P. J., D. J. Delene, and J. A. Ogren, 2001: Four years of continuous surface aerosol measurements from the Department of energy's atmospheric radiation measurement program southern great plains cloud and radiation testbed site. *J. Geophys. Res*., **106**, 20 735–20 747, https://doi.org/10.1029/2001jd000785.

Sheridan, P. J., A. Jefferson, and J. A. Ogren, 2002: Spatial variability of submicrometer aerosol radiative properties over the Indian Ocean during INDOEX. *J. Geophys. Res*., **107**, 8011, https://doi.org/10.1029/2000jd000166.

Tao, J. C., C. S. Zhao, Y. Kuang, G. Zhao, C. Y. Shen, Y. L. Yu, Y. X. Bian, and W. Y. Xu, 2018: A new method for calculating number concentrations of cloud condensation nuclei based on measurements of a three-wavelength humidified nephelometer system. *Atmospheric Measurement Techniques*, **11**, 895–906, https://doi.org/10.5194/amt-11-895-2018.

Titos, G., H. Lyamani, A. Cazorla, M. Sorribas, I. Foyo-Moreno, A. Wiedensohler, and L. Alados-Arboledas, 2014: Study of the relative humidity dependence of aerosol light-scattering in southern Spain. *Tellus B: Chemical and Physical Meteorology*, **66**, 24536, https://doi.org/10.3402/tellusb.v66.24536.

Titos, G., A. Cazorla, P. Zieger, E. Andrews, H. Lyamani, M. J. Granados-Muñoz, F. J. Olmo, and L. Alados-Arboledas, 2016: Effect of hygroscopic growth on the aerosol light-scattering coefficient: A review of measurements, techniques and error sources. *Atmos. Environ*., **141**, 494–507, https://doi.org/10.1016/j.atmosenv.2016.07.021.

Wang, W., M. J. Rood, C. M. Carrico, D. S. Covert, P. K. Quinn, and T. S. Bates, 2007: Aerosol optical properties along the northeast coast of North America during the New England air quality study-intercontinental transport and chemical transformation 2004 campaign and the influence of aerosol composition. *J. Geophys. Res*., **112**, D10S23, https://doi.org/10.1029/2006jd007579.

WMO/GAW, 2003: Aerosol measurement procedures, guidelines and recommendations. GAWRep. 153. World Meteorol. Organ., Geneva, Switzerland. Available from https://library.wmo.int/index.php?lvl=notice_display&id=11085#.XO-Jg_m-BN9.

Wu, Y. F., and Coauthors, 2017: Investigation of hygroscopic growth effect on aerosol scattering coefficient at a rural site in the southern North China Plain. *Science of the Total Environment*, **599–600**, 76–84, https://doi.org/10.1016/j.scitotenv.2017.04.194.

Yan, P., X. L. Pan, J. Tang, X. J. Zhou, R. J. Zhang, and L. M. Zeng, 2009: Hygroscopic growth of aerosol scattering coefficient: A comparative analysis between urban and suburban sites at winter in Beijing. *Particuology*, **7**, 52–60, https://doi.org/10.1016/j.partic.2008.11.009.

Yang, Y. R., and Coauthors, 2015: Characteristics and formation mechanism of continuous hazes in China: A case study during the autumn of 2014 in the North China Plain. *Atmospheric Chemistry and Physics*, **15**, 8165–8178, https://doi.org/10.5194/acp-15-8165-2015.

Yu, Y. L., C. S. Zhao, Y. Kuang, J. C. Tao, G. Zhao, C. Y. Shen, and W. Y. Xu, 2018: A parameterization for the light scattering enhancement factor with aerosol chemical compositions. *Atmos. Environ.*, **191**, 370–377, https://doi.org/10.1016/j. atmosenv.2018.08.016.

Zhang, L., and Coauthors, 2015: Observations of relative humidity effects on aerosol light scattering in the Yangtze River Delta of China. *Atmospheric Chemistry and Physics*, **15**, 8439–8454, https://doi.org/10.5194/acp-15-8439-2015.

Zhao, G., C. S. Zhao, Y. Kuang, Y. X. Bian, J. C. Tao, C. Y. Shen, and Y. L. Yu, 2018a: Calculating the aerosol asymmetry factor based on measurements from the humidified nephelometer system. *Atmospheric Chemistry and Physics*, **8**, 9049–9060, https://doi.org/10.5194/acp-18-9049-2018.

Zhao, P. S., J. Ding, X. Du, and J. Su, 2018b: Hygroscopic growth effect on aerosol light scattering in the urban area of Beijing: A long-term measurement by a wide-range and high-resolution humidified nephelometer system. *Atmospheric Chemistry and Physics Discussions*, 1–22, https://doi.org/10.5194/acp-2018-794.

Zieger, P., and Coauthors, 2014: Influence of water uptake on the aerosol particle light scattering coefficients of the Central European aerosol. *Tellus B*: *Chemical and Physical Meteorology*, **66**, 22716, https://doi.org/10.3402/tellusb.v66.22716.